FULL WAVE CALCULATION FOR A GAUSSIAN VLF WAVE INJECTION INTO THE IONOSPHERE

Isamu NAGANO, Masayoshi MAMBO, Shigeo YOSHIZAWA,

Department of Electrical Engineering, Kanazawa University, 40–20, Kodatsuno 2-chome, Kanazawa 920

Iwane KIMURA

Department of Electrical Engineering, Kyoto University, Sakyo-ku, Kyoto 606

and

Hisao YAMAGISHI

National Institute of Polar Research, 9–10, Kaga 1-chome, Itabashi-ku, Tokyo 173

Abstract: Both spatial distributions of the field intensity and the polarization at the ground of a spatially confined whistler mode wave, which has a Gaussian amplitude incident onto the ionosphere from above are computed by a full wave method. The propagation paths in the earth-ionosphere wave guide are estimated by tracing the peaks of these wave distributions at different altitudes.

From these calculations, the following interesting results are obtained:

(1) The spatial attenuation rate of the wave intensity in the earth-ionosphere wave guide mode is about −10 dB/100 km for a distance less than a few hundred kilometers from the source.

(2) The polarization is right-handed circular just underneath the source point, but it becomes left handed at some distance away.

1. Introduction

In the recent years, multi-station simultaneous observations of natural VLF waves and artificially transmitted VLF signals have been carried out on the ground by TSURUDA *et al.* (1981). They reported that the amplitude observation of a signal, transmitted from Siple in Antarctica and propagated to the northern hemisphere through the whistler mode, revealed a high spatial attenuation in the space below the ionosphere. Natural VLF emissions associated with auroral arcs have been observed over a relatively small area on the ground below the ionospheric exit point of the waves (MAKITA, 1979). It is not possible to support these experimental results theoretically with an approximate treatment using the wave guide mode theory (WALKER, 1974).

In order to estimate the precise quantitative amplitudes of the signals at any ionospheric level from these actually observed on the ground, it is necessary to establish a full wave technique which makes it possible to treat a spatially confined wave packet instead of a plane wave.

In this paper, a numerical calculation technique is developed to solve these pro-

blems by using the full wave method. A whistler mode wave incident onto the ionosphere from above is assumed to be a two-dimensional Gaussian beam wave which is represented as a superposition of a number of elementary plane waves. For each elementary plane wave we calculate the field components in the ionosphere by the full wave method, and can obtain the field distribution at an arbitrary altitude by synthesizing the full wave solutions from all initial elementary plane waves.

For the practical computation of the downgoing whistler mode Gaussian beam waves, an electron density model for the lower ionosphere is adopted which is an experimental profile observed by a sounding rocket at Syowa Station. The field distributions on the ground are calculated for various scales of the spatially confined incident wave and their virtual propagation characteristics are discussed (*e.g.* transmission cone angle and angle of emittance). Finally the distribution of polarization on the ground is presented.

2. Basic Theory

Our method is based on the expansion of a spatially confined electromagnetic wave into an infinite set of plane waves. It is assumed that the time variation is represented by $e^{j\omega t}$. A Cartesian coordinate system (x, y, z) is used as shown in Fig. 1. For simplicity, we consider a two-dimensional beam wave which is constant along the y-axis and has a spatially confined amplitude distribution in the x-direction. Under these conditions the electromagnetic fields of the beam wave, $\boldsymbol{E}(x, z)$ and $\mathscr{H}(x, z)$ ($\equiv Z_0 H$ where Z_0 is the wave impedance in free space), are expressed as follows:

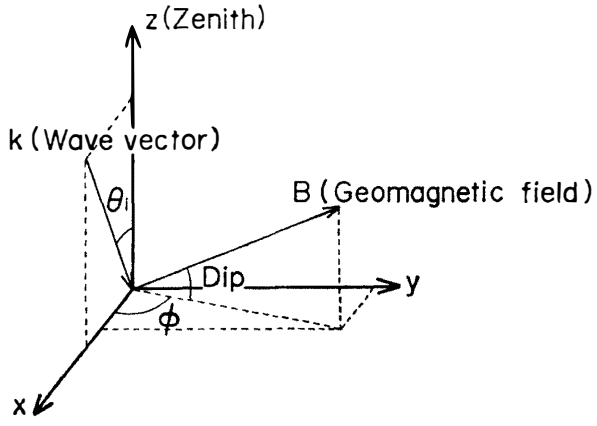

Fig. 1. The coordinate system.

$$\begin{aligned}\boldsymbol{E}(x, z)&=\frac{1}{2\pi}\int_{-\infty}^{\infty}\tilde{\boldsymbol{E}}(k_x, z)e^{-jk_x x}\mathrm{d}k_x\\ \mathscr{H}(x, z)&=\frac{1}{2\pi}\int_{-\infty}^{\infty}\tilde{\mathscr{H}}(k_x, z)e^{-jk_x x}\mathrm{d}k_x\,,\end{aligned}\tag{1}$$

where $\sim$ denotes the Fourier spectrum component, *i.e.*,

$$\begin{aligned}\tilde{\boldsymbol{E}}(k_x, z)&=\int_{-\infty}^{\infty}\boldsymbol{E}(x, z)e^{jk_x x}\mathrm{d}x\\ \tilde{\mathscr{H}}(k_x, z)&=\int_{-\infty}^{\infty}\mathscr{H}(x, z)e^{jk_x x}\mathrm{d}x\,,\end{aligned}\tag{2}$$

where k_x is the x-component of the wave normal vector $\boldsymbol{k}$ and $k_x=k_0 n \sin\theta_i$ (k_0 is wave number in free space, n is the refractive index at the altitude of incidence, θ_i is the angle of incidence).

Regarding the ionosphere as a horizontally stratified medium in the coordinates shown in Fig. 1, an elementary plane wave which is a component of the spatially confined beam wave in eq. (1) satisfies the following equation (NAGANO *et al.*, 1975):

$$\frac{d\tilde{\boldsymbol{e}}}{dz}=-j\,k_0\boldsymbol{T}(k_x, z)\tilde{\boldsymbol{e}}\,, \tag{3}$$

where $\tilde{\boldsymbol{e}}=(\tilde{E}_x, -\tilde{E}_y, \tilde{\mathscr{H}}_x, \tilde{\mathscr{H}}_y)^t$, ($t$ denoting the transpose of the vector), and $\boldsymbol{T}$ is a 4×4 matrix depending on the incident wave normal and the constitution of the medium. In the following a cold plasma approximation is used for the medium.

Equation (3) can be solved by a full wave method. Therefore we can obtain the full wave solutions of an elementary plane wave with a unit amplitude at the beginning, corresponding to each wave number k_x which will be given by the initial condition. If we express this solution as $\tilde{F}(k_x, z)$, the electric field of eq. (1) is rewritten as

$$E(x, z)=\frac{1}{2\pi}\int_{-\infty}^{\infty} C_1(k_x)\tilde{F}(k_x, z)e^{-jk_x x}dk_x\,, \tag{4}$$

where $C_1(k_x)$ is a function determined by the initial amplitude distribution of the beam wave. The magnetic field is also given by a similar expression, although we will not use it here.

Now we express the spatial amplitude distribution of a downgoing wave at the incident altitude as the function of x, $g(x)$, which is expanded into a set of plane waves by Fourier integral,

$$g(x)=\frac{1}{2\pi}\int_{-\infty}^{\infty}\tilde{G}(k_x)e^{-jk_x x}dk_x\,, \tag{5}$$

$$\tilde{G}(k_x)=\int_{-\infty}^{\infty} g(x)e^{jk_x x}dx\,. \tag{6}$$

Then eq. (4) must be equal to eq. (5) at the incident altitude, thereby eq. (4) becomes

$$E(x, z)=\frac{1}{2\pi}\int_{-\infty}^{\infty}\tilde{G}(k_x)\tilde{F}(k_x, z)e^{-jk_x x}dk_x\,. \tag{7}$$

In this way we can obtain the exact solution of the beam wave by integrating the full wave solutions at arbitrary altitudes.

The procedures for the numerical calculation of eq. (7) are carried out as follows:

(1) The spatial amplitude distribution of the downgoing wave $g(x)$ is assumed at the altitude of incidence. In this case we can choose $g(x)$ as a Gaussian type function so as to be able to calculate eq. (6) analytically.

(2) Equation (7) is approximated by summing up a finite number of k_x, up to a few hundred points, instead of integrating an infinite number of k_x. In order to increase the accuracy for such a finite approximation, we use the Discrete Fourier Transform (DFT) method.

(3) The full wave solution $\tilde{F}(k_x, z)$ is calculated by the multi-layered method

for each elemental plane wave with a wave number of k_x. Thereby we can calculate the spatial distribution $E(x, z)$ at an arbitrary altitude using eq. (4).

3. Model for Calculation

3.1. A model for the incident beam wave

The amplitude distribution of a downgoing whistler wave is assumed to be of the following form at the incident altitude.

$$g(x)=\exp\left(-\frac{x^2}{2\sigma^2}-jk_{x0}x\right), \tag{8}$$

where σ is a factor of the beam width, and k_{x0} is the x-component of the wave normal vector, which is represents a central direction of propagation of the beam wave. The Fourier integral of eq. (8) can be calculated analytically as follows:

$$\tilde{G}(k_x)=(2\pi)^{1/2}\sigma\exp\left(-\frac{1}{2}\sigma^2(k_x-k_{x0})^2\right). \tag{9}$$

These eqs. (8) and (9) are both Gaussian type functions, therefore we call such a beam wave the Gaussian beam wave.

3.2. Lower ionospheric model

The lower ionospheric model used in the numerical calculations is shown in Fig. 2. We have used the electron density profile which was observed by the S-210JA-22 rocket launched at Syowa Station when the ionosphere was in a relatively quiet condition (OGAWA *et al.*, 1976). Also we have adopted the atmospheric pressure for a latitude of 70°N in December (COSPAR, 1972). An effective collision frequency profile ν_{eff} is derived from a mono-energetic collision frequency ν_m which is proportional to the atmospheric pressure (THRANE and PIGGOTT, 1966). MIYAZAKI estimated the collision frequency from the Cosmic Noise Absorption (CNA) data observed at Syowa Station (MIYAZAKI, 1975). Our model of the collision frequency profile is in good agreement with his estimation.

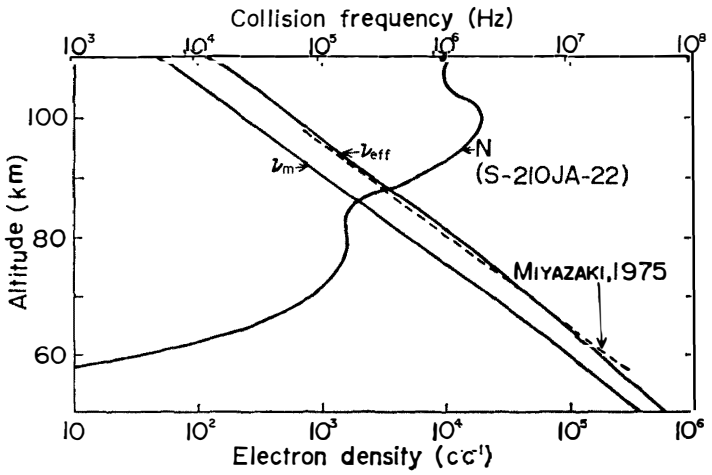

Fig. 2. The electron density and the collision frequency profiles used in the numerical calculation.

4. Calculated Results and Discussion

In this section the wave magnetic fields which we expected to be observed at the ground are computed and discussed for various cases. A change of the polarization depending upon the distance along the ground from beneath the exit point is also discussed. The incident wave, which is of the whistler mode with a right-handed polarization, is assumed to have a Gaussian distribution in the x-direction in the horizontal plane at the topside boundary of the lower ionosphere. In this full wave method, the ground reflection effect is considered (NAGANO *et al.*, 1980). The topside boundary of the ionosphere is assumed to be located at an altitude of 110 km, and the free space is assumed below an altitude of 50 km. The schematic structure of our problem is shown in Fig. 3. The other parameters used in the numerical calculation are shown in Table 1.

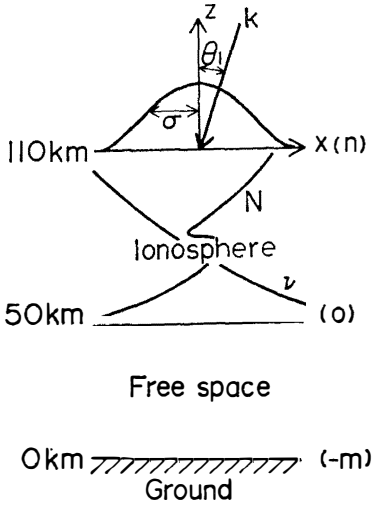

Fig. 3. The schematic structure of the problem.

Table 1. Parameters used in the numerical calculations.

Wave frequency	f	3.0, 5.0, 8.0 (kHz)
Angle of incidence	θ_i	$0°\sim 7°$
The beam width of the incident wave	σ	$\lambda\sim 15\lambda$ (λ; the wave length at incident level)
Azimuth angle	ϕ	0° (North-South propagation)
Geomagnetic dip angle	dip	70°
Electron gyro frequency	f_H	1.244 (MHz)
The conductivity and dielectric constant of the Earth		10^{-3} (S/m) and 10

4.1. Transmission cone angle of the beam wave

Figure 4 shows the relationship between the incident angle of the downgoing whistler wave and the maximum amplitude of the beam wave on the ground, where θ_p denotes the transmission cone angle calculated by Snell's law. As is seen in Fig. 4, the effective transmission cone angle for the Gaussian beam wave is a little wider than that for the plane wave, becoming wider as the beam width σ becomes narrower. This result is explained by the distribution of the angular spectra constituting the beam wave. That is, even if the main central direction of the incident beam wave is outside of the transmission cone θ_p, a part of the distributed angular spectra would still remain inside the cone, so that the intensity level of the beam wave outside the transmission cone θ_p on the ground becomes much stronger than that for the plane wave case. Since the variance of the angular spectrum function becomes greater as σ becomes narrower, the effective transmission cone angle becomes wider, and the maximum amplitude of the wave at the ground becomes smaller than that of the plane wave case, for small incident angles.

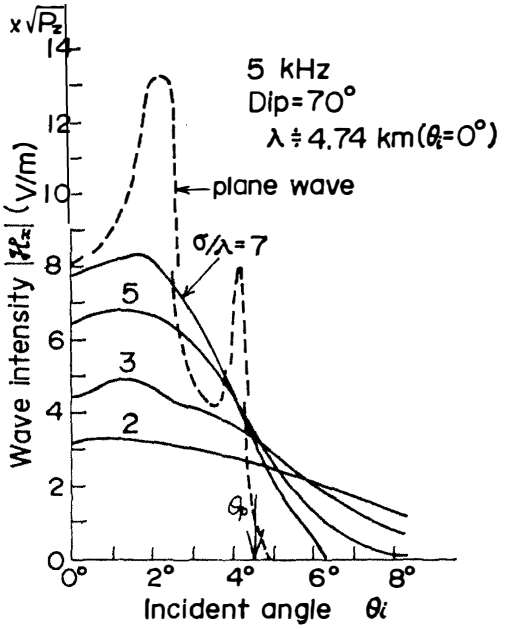

Fig. 4. The maximum amplitude of the wave field at the ground versus the incident angle for various beam widths of the incident wave (σ/λ). The vertical axis is normarized by the square root of z component of the Poynting flux (W/m^2) of the incident whistler mode wave. θ_p denotes the angle of transmission cone derived by Snell's law.

4.2. The ray path and the angle of emittance

Estimation of the ray paths of the downgoing whistler mode wave in the earth-ionosphere wave guide is an important problem for finding the exit point from the ionosphere.

The ray path in the earth-ionosphere wave guide is calculated by the following process:

(1) Spatial distributions of the wave at several altitudes in free space are computed.

(2) The upgoing and downgoing waves are separated.

(3) Ray paths of these waves are defined as the loci of the points of maximum amplitude of the waves at different altitudes.

Figure 5 shows the ray paths of the upgoing and downgoing waves in the earth-ionosphere wave guide. The second and third peaks of waves at the ground are obviously identified as the interference pattern of the upgoing and downgoing waves reflected both in the ionosphere and at the ground surface.

We define the angle of emittance as the angle between z-axis and the direction of the downgoing waves at the exit point of the ionosphere.

Figure 6 shows the relationship between the angle of emittance and $n \sin \theta_i$ for different widths of the incident beam wave. The angle of emittance at the exit point has a saturation characteristics when the width of the beam wave is less than ten wave lengths as shown in Fig. 6, and the maximum angle becomes smaller in proportion to the width of the beam. It turns out from these numerical results that if the elevation angle of the arriving VLF waves observed by the direction finder on the ground is less than sixty degrees, the spatial distribution of the downgoing wave at the incident altitude may be as wide as 15λ, where λ denotes the wave length at the incident altitude.

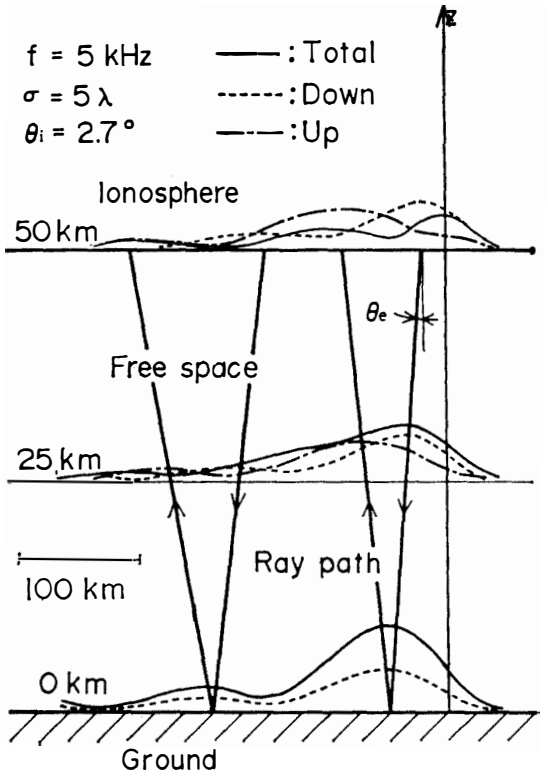

Fig. 5. The ray path of the upgoing and downgoing waves in the earth-ionosphere wave guide. θ_e denotes the angle of emittance of the downgoing wave. The solid, broken and chained curves show the distribution of the total wave, downgoing and upgoing waves, respectively.

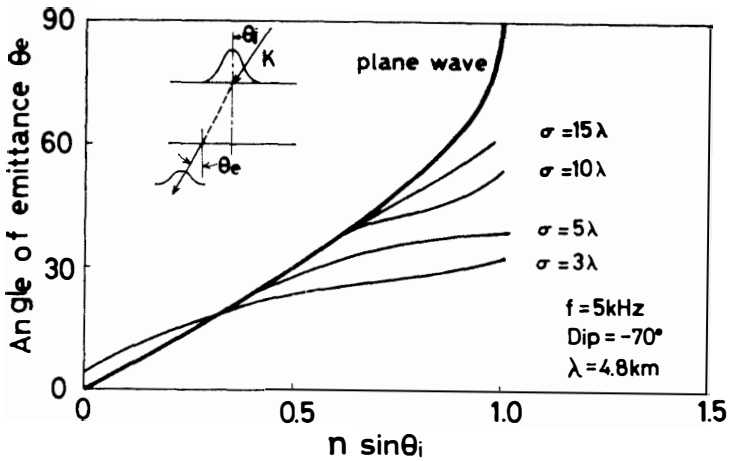

Fig. 6. The angle of emittance θ_e versus $n \sin \theta_i$ for various values of the beam width σ of the incident wave. The curve labeled 'plane wave' shows the value calculated by Snell's law. n is the refractive index at the incident level.

4.3. Field intensity dependence on the beam width of the incident wave

We calculate the wave fi eldintensity on the ground for various beam widths of the vertical incident wave and examine how the distribution of the fi eldon the ground is dependent on the beam width of the incident wave. Although the resultant shape of the distribution of the wave on the ground is slightly different from the Gaussian form assumed at the incident altitude, we introduce the equivalent quantity σ_g to express the width of the distribution of the wave fi eldat the ground. The value of σ_g

is defined as the distance in λ from the point of maximum amplitude to the points of amplitude equal to $e^{-1/2}$ of its value.

Figure 7 shows the maximum amplitude and the equivalent width of the wave field at the ground *versus* the beam width of the incident wave. As is seen in the broken curve of Fig. 7, the beam width of the ground wave becomes about 15λ and is independent of that of the incident wave when $\sigma<2\lambda$. It means that the angular spectra of incident beam wave is distributed uniformly within the transmission cone angle.

On the other hand, the maximum intensity of the wave field becomes small compared to that of the plane wave as the incident beam width becomes less than 8λ.

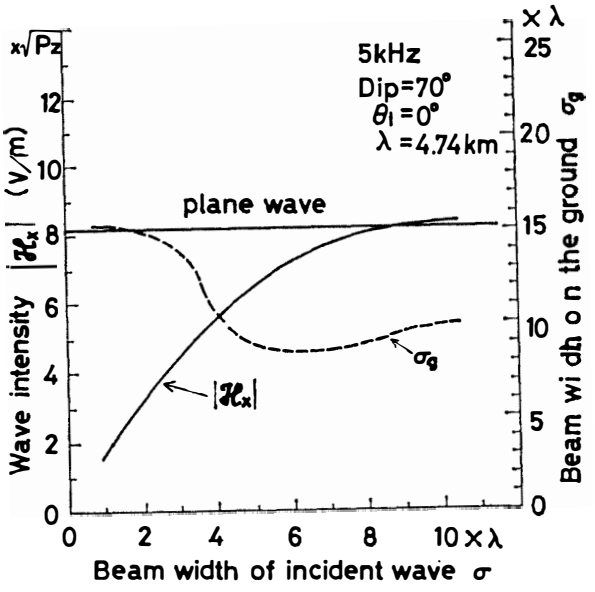

Fig. 7. The maximum amplitude and the equivalent beam width at the ground versus the beam width of the incident wave. The scales for the solid and broken curves correspond to the vertical axes at the right and left handed sides, respectively.

4.4. Spatial attenuation of the wave field on the ground

In order to estimate the spatial attenuation on the ground, it is assumed that the angular spectra of the downgoing whistler mode wave incident onto the ionosphere is spread over the transmission cone angle. Such a incident wave corresponds to a Gaussian beam wave with $\sigma<2\lambda$ as stated in the previous section. Therefore, the computations in this section are performed under the conditions of $\sigma=\lambda$ and $\theta_i=0°$.

Figures 8a, 8b and 8c show the spatial distributions for three different frequencies calculated by our method. The computed wave field included the effect of the multi-reflection in the earth-ionosphere wave guide. The x- and y-components of the magnetic field $\mathscr{H}$ correspond to the TE and TM modes in free space, respectively. The attenuation rate is about -20 dB/500 km as an average over a long distance and locally is greater than -10 dB/100 km in both cases of frequencies of 5 kHz and 8 kHz.

WALKER (1974) calculated analytically the spatial amplitude distribution of the VLF waves which were originally incident onto the ionosphere from above, for a model three layered medium representing the earth-free space-ionosphere. He obtained an attenuation rate of a few tens dB per 1000 km in free space under the ionosphere. However, according to multi-station ground based observations of one hop whistler

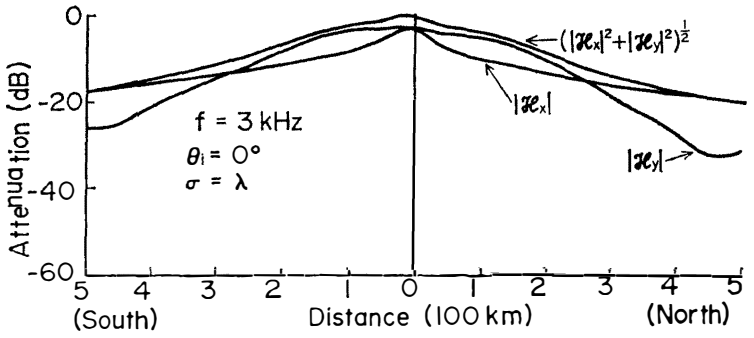

Fig. 8a.

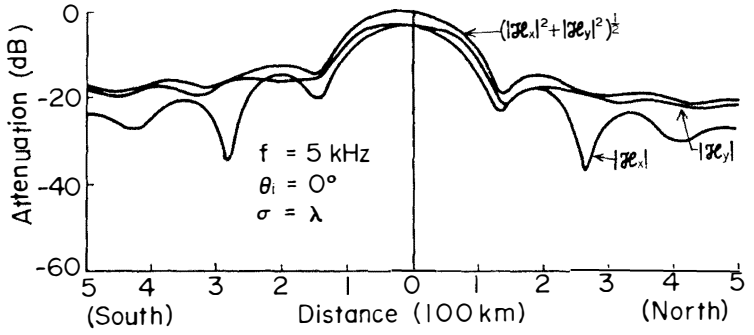

Fig. 8b.

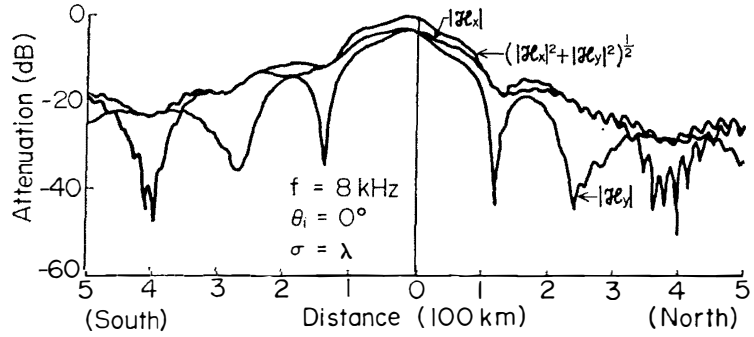

Fig. 8c.

Fig. 8. The spatial distributions of the downgoing whistler mode wave on the ground at vertical incidence. a. f=3 kHz; b. f=5 kHz; c. f=8 kHz.

mode waves of the Siple transmission near the conjugate point of Siple station (TSURUDA *et al.*, 1981), it was found that the spatial attenuation rate is sometimes much steeper (—7 dB/100 km) than the theoretical value obtained by WALKER.

Our results are extremely different from the value obtained by the wave guide mode theory (WALKER, 1974; HELLIWELL, 1965), but are in good agreement with the experimental results reported by TSURUDA *et al.* (1981).

4.5. Polarization on the ground

We can easily recognize that the polarization at the ground will change because of the variation of the amplitude ratio $|\mathscr{H}_x|$ to $|\mathscr{H}_y|$ as shown in Fig. 8. We have computed the polarization parameter from the three components of the magnetic field ($\mathscr{H}_x$, $\mathscr{H}_y$, $\mathscr{H}_z$) as shown in Figs. 9a, 9b and 9c (MEANS, 1972). This parameter denotes the ratio of the major axis to the minor axis of the ellipse in the plane perpendicular to the wave normal. As is seen in Fig. 9, polarization in the left handed sense

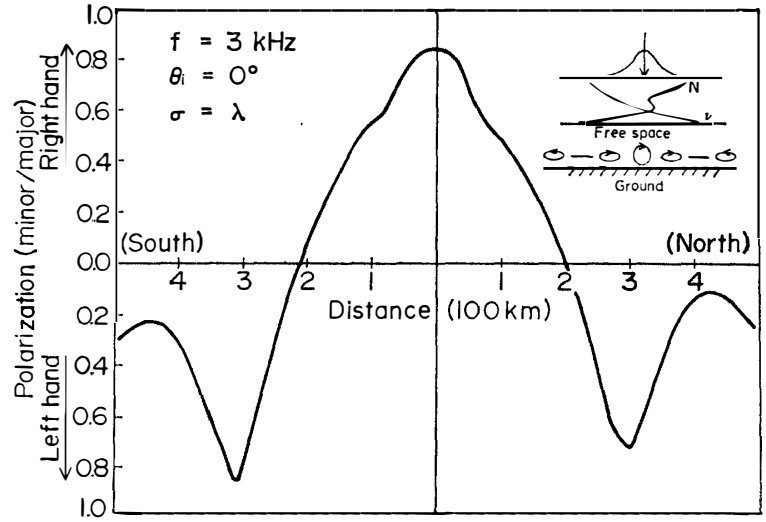

Fig. 9a.

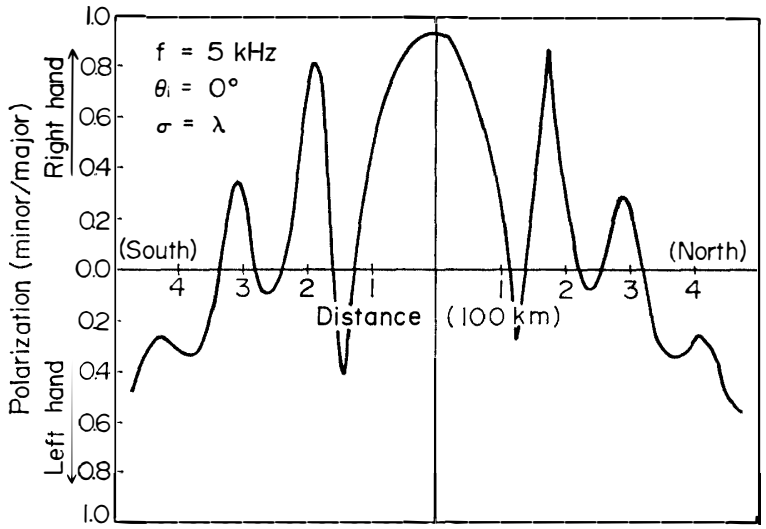

Fig. 9b.

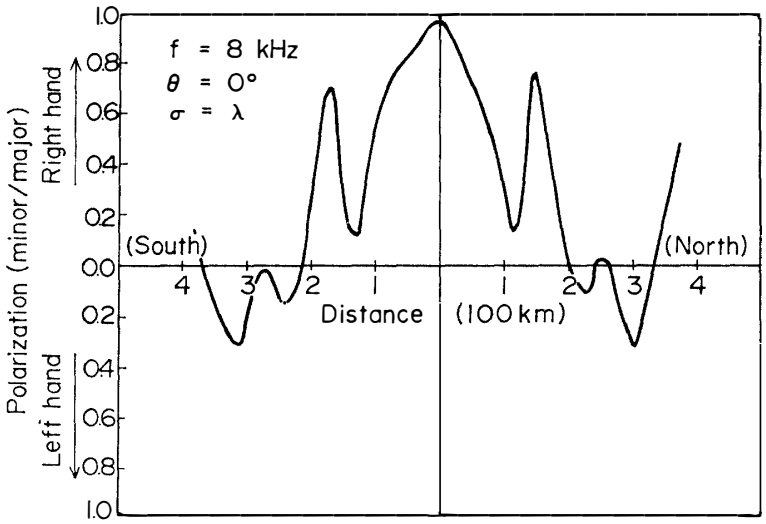

Fig. 9c.

Fig. 9. Variation of the polarization versus the distance from the point directly below the incident beam wave (refer to Fig. 8). a. f=3 kHz; b. f=5 kHz; c. f=8 kHz.

appears at distances greater than 100 km from the ionospheric exit point of the wave. In this case, the polarization parameter corresponds to the conventional definition of the polarization P (TSURUDA *et al.*, 1979), because the amplitude of the $\mathscr{H}_z$ component on the ground is very small.

5. Conclusion

The full wave treatment has been developed for the spatially confined downgoing whistler mode wave incident onto the ionosphere from above. The major points we have discussed in this paper are as follows:

(1) The effective transmission cone angle of beam waves is somewhat wider than that of the plane wave case.

(2) The angle of emittance of the beam wave tends to become smaller than that calculated simply by Snell's law.

(3) The attenuation rate determined from the spatial distribution of the signal amplitude below the ionosphere is much greater than that theoretically obtained by the mode theory.

(4) The transmitted wave on the ground shows a right-handed polarization in the vicinity of the exit point, but a left-handed components appears at greater distances.

This full wave method is applicable for analyzing the spatial distribution of natural VLF emissions observed on the ground by a multi-station network and becomes a powerful tool for examining the accuracy of the various types of direction finding systems.

Acknowledgments

The authors wish to express their thanks to Prof. T. HIRASAWA and Dr. H. FUKUNISHI for supporting this study. We are also grateful to Dr. K. TSURUDA and Dr. K. MAKITA for their helpful advice.

References

COSPAR (1972): COSPAR International Reference Atmosphere, ed. by A. C. STICKLAND. Berline, Acadimie, 202 p.

HELLIWELL, R. A. (1965): Whistler and Related Ionospheric Phenomena. Stanford, Stanford Univ. Press, 349 p.

MAKITA, K. (1979): VLF-LF hiss emissions associated with aurora. Mem. Natl Inst. Polar Res., Ser. A, **16**, 126 p.

MEANS, J. D. (1972): Use of the three-dimensional covariance matrix in analyzing the polarization properties of plane waves. J. Geophys. Res., **77**, 5551–5559.

MIYAZAKI, S. (1975): Relation between lower ionospheric electron density profiles and cosmic noise absorption during auroral zone disturbances. J. Geomagn. Geoelectr., **27**, 113–129.

NAGANO, I., MAMBO, M. and HUTATSUISHI, G. (1975): Numerical calculation of electromagnetic waves in anisotropic multi-layered medium. Radio Sci., **10**, 611–617.

NAGANO, I., MAMBO, M., YAMAKAWA, H. and KIMURA, I. (1980): Kyokkô-tai ni okeru VLF-ha no furu uêbu keisan (A full wave calculation of VLF waves in auroral zone). Nankyoku Shiryô (Antarct. Rec.), **68**, 302–214.

OGAWA, T., MORI, H. and MIYAZAKI, S. (1976): Nankyoku roketto S-210JA-22 to S-310JA-1 ni yoru denshi mitsudo ondo no kansoku (A observation of the electron density and the temperature by the rockets S-210JA-22 and S-310JA-1). Chikyû Denjiki Gakkai (J. Geomagn. Geoelectr.), II-22.

THRANE, E. V. and PIGGOTT, W. R. (1966): The collision frequency in the *E*- and *D*-regions of the ionosphere. J. Atmos. Terr. Phys., **28**, 721–737.

TSURUDA, K. and IKEDA, M. (1979): Comparison of three different types of VLF direction-finding techniques. J. Geophys. Res., **84A**, 5325–5332.

TSURUDA, K. and MACHIDA, S. (1981): Multi-station observation of VLF chorus and Siple triggered emissions. Paper presented at US-Japan seminar on wave particle interactions in space plasma, held at Kyoto, Japan.

WALKER, A. D. M. (1974): Excitation of earth-ionosphere waveguide by downgoing whistlers. Proc. R. Soc. Lond., A, **340**, 367–393.

(Received October 30, 1981; Revised manuscript received December 25, 1981)